Highly Enhanced Selectivity and Easy Regeneration for the Separation of CO2 over N-2 on Melamine-Based Microporous Organic Polymers

ARTICLE *in* INDUSTRIAL & ENGINEERING CHEMISTRY RESEARCH · JULY 2014

Impact Factor: 2.59 · DOI: 10.1021/ie501736t

I&EC research
Industrial & Engineering Chemistry Research

Article

pubs.acs.org/IECR

Highly Enhanced Selectivity and Easy Regeneration for the Separation of CO_2 over N_2 on Melamine-Based Microporous Organic Polymers

Jing-Xiu Hu,[†] Hao Shang,[†] Jin-Gui Wang,[‡] Liang Luo,[§] Qiang Xiao,*[,†,∥] Yi-Jun Zhong,[†] and Wei-Dong Zhu[†]

[†]Key Laboratory of the Ministry of Education for Advanced Catalysis Materials, Institute of Physical Chemistry, Zhejiang Normal University, 321004 Jinhua, P. R. China

[‡]Division of Chemistry and Biological Chemistry, School of Physical and Mathematical Sciences, Nanyang Technological University, 21 Nanyang Link, Singapore 637371, Singapore

[§]Discovery Pharmaceutics, Bristol-Myers Squibb Company, 5 Research Parkway, Wallingford, Connecticut 06492, United States

[∥]Key Laboratory of Advanced Energy Materials Chemistry (Ministry of Education), Collaborative Innovation Center of Chemical Science and Engineering (Tianjin), College of Chemistry, Nankai University, 300071 Tianjin, P. R. China

Supporting Information

ABSTRACT: Melamine based microporous organic polymers (MBMOPs) have been prepared via a one-pot polymerization using the Schiff base reaction. Various techniques such as FT-IR, Ar adsorption, SEM, TEM, and TG have been used to characterize the textural structure, porosity, and stability of the synthesized MBMOPs. The adsorption isotherms of CO_2 and N_2 on MBMOPs have been accurately measured at pressures up to 118 kPa and different temperatures. Ascribed to the specific affinity of amine groups for CO_2, the robust microporous MBMOPs display excellent CO_2 adsorption performance in terms of both capacity, up to 2.8 mmol g^{-1} at 273 K and 118 kPa, and selectivity over N_2. Dual-site Langmuir (DSL) or single-site Langmuir (SSL) model describes well the equilibrium data for the adsorption of CO_2 or N_2 on MBMOPs, respectively. The binary gas adsorption isotherms predicted by the ideal adsorbed solution theory (IAST) show that the prepared MBMOPs exhibit very high selectivities for CO_2 over N_2, up to 83.7, for equimolar mixtures of CO_2 and N_2 at 298 K and 100 kPa. The dynamic CO_2 adsorption capacity and selectivity against N_2 over MBMOPs have been experimentally investigated by breakthrough column technique at 1 bar and 298 K, indicating that a complete separation is available. Remarkably, CO_2 capture−regeneration experiments indicate that MBMOPs can be easily regenerated by only purging with He or N_2 rather than by raising the temperature, suggesting that MBMOPs are promising candidates of pressure swing adsorption (PSA) adsorbents for the separation of CO_2−N_2.

1. INTRODUCTION

The control of carbon dioxide (CO_2) emission has aroused people's great concern due to the gradual increase in the atmospheric concentration of CO_2 and the consequential global climate changes resulting from the excessive consuming of fossil fuel.[1] Postcombustion CO_2 capture and air separation are important potential approaches to reduce CO_2 emission to the atmosphere and integral parts of the energy industry.[2] Although conventional chemical absorption based on alkanolamine solvents such as monoethanolamine can capture CO_2 effectively, they have severe corrosion problems and also are highly energy-consuming because of the energy penalty necessary for regenerating.[3,4] Pressure swing adsorption (PSA) and temperature swing adsorption (TSA) using solid adsorbents are some of the common techniques that could be applicable for removal of CO_2 from fuel gas stream.[5] Various physical absorbents such as zeolite[6] and mesoporous silica[7,8] have been intensively investigated as candidates for CO_2 capture and sequestration from flue gas by physisorption. However, these adsorbents were limited by low adsorption capacity, low selectivity, and moisture sensitivity.[6] To enhance adsorption capacity and selectivity of adsorbent, recently, many researchers focus on grafting amines or introducing polymers with amino groups onto nanoporous and mesoporous adsorbents.[9−16] These amino functionalized materials commonly could take advantage of high CO_2 capacity and selectivity. However, these amino functionalized adsorbents encounter some drawbacks from the viewpoint of application, mainly their difficult regeneration and poor stability.[14,17] This type of adsorbents can only find applications in the TSA process, which features high energy consumption and a low handling capacity compared with PSA.

Metal−organic frameworks (MOFs) with remarkable properties, including large specific surface area (>5000 m^2 g^{-1}), abundant porosity (up to 2 cm^3 g^{-1}), high physical and chemical stability, low skeleton density, flexible chemical modification, have been claimed as potential CO_2 adsorb-

Received: April 28, 2014
Revised: June 30, 2014
Accepted: July 1, 2014
Published: July 1, 2014

dx.doi.org/10.1021/ie501736t | Ind. Eng. Chem. Res. 2014, 53, 11828−11837

ents.[18−23] Large CO_2 adsorption capacities on MOFs have been found, e.g., 33.5 mmol g^{-1} (at 298 K, 32 bar) on MOF-177,[21] 40 mmol g^{-1} (at 298 K, 50 bar) on MIL-101(Cr).[24] In spite of the high CO_2 uptake amount at high pressures, the amount and selectivity for CO_2 adsorption on MOFs especially at low partial pressures still need to be improved to a great extent.[25−27]

Recently, porous organic frameworks (POFs) formed by organic polymerization method, such as porous aromatic frameworks (PAFs),[28−30] conjugated microporous polymers,[31,32] and covalent organic frameworks (COFs),[33] have emerged as good candidates for CO_2 capture and sequestration.[34,35] With ultrahigh specific surface area (up to 6000 m^2 g^{-1}), large pore volume, and pure organic framework composed of versatile buildings, POFs exhibit very large CO_2 adsorption amount at high pressures, e.g., 29.6 mmol g^{-1} on PAF-1[29] (at 40 bar, 298 K) and 38.9 mmol g^{-1} on PPN-4[36] (at 50 bar, 298 K). However, the adsorption potential of CO_2 on such POFs is fairly low because of the lack of functional groups with affinity to CO_2. As a result, at ambient pressures, the CO_2 adsorption on POFs is dramatically reduced. For instance, the CO_2 uptake of PAF-1 is about 1.1 mmol g^{-1} at 1 bar and 298 K.[29]

CO_2 adsorption in slit carbon pores investigated using GCMC and NLDFT reveals that 1 nm is the upper limit of sensitivity for the subatmospheric CO_2 adsorption at 273 K into the pore sizes.[37] In other words, suitable pore sizes less than 1 nm are required for CO_2 adsorption at ambient conditions. Qiu's group reported two types of microporous POFs, JUC-Z4 and JUC-Z5, which exhibit CO_2 adsorptions of 1.7 and 1.5 mmol g^{-1} at 298 K and 1 bar, respectively, showing an enhancement of CO_2 adsorption amounts in comparison to PAF-1.[30] Another strategy is to incorporate specific functional groups such as amine or azo group in order to tune the isosteric heats of adsorption for CO_2.[34,38] Lu et al. reported an amine-grafted porous polymer networks for CO_2 capture from air, which shows an extraordinarily high CO_2 selectivity (3.6×10^{10}) and loading capacity (1.04 mmol g^{-1}). Moreover, the presence of azo groups in network (azo-COPs) could also greatly enhance CO_2 selectivity by N_2 phobicity.[39]

On the basis of the above-mentioned discussion, melamine-based microporous organic polymer (MBMOP) synthesized via the Schiff base chemistry comes into our sight.[40,41] Ascribed to the abundant microporosity and plenty of amine groups, MBMOPs exhibit good CO_2 capture properties.[42,43] However, to the best of our knowledge, no investigation on the binary adsorption of CO_2−N_2 and CO_2 adsorption−desorption cycle on MBMOPs, which is quite related to their separation properties, has been reported to date.

In this study, we synthesized MBMOPs via Schiff base reaction using different phthalaldehyde analogues as building blocks. The adsorption behaviors of CO_2 and N_2 on the prepared MBMOPs were systematically investigated. The synthesized MBMOPs exhibit an excellent CO_2 adsorption performance in terms of high CO_2 adsorption capacity, good CO_2 selectivity over N_2, and more importantly easy regeneration. These merits endow MBMOPs a good prospect as PSA candidate adsorbents for the separation of CO_2−N_2 mixture.

2. EXPERIMENTAL SECTION

2.1. Materials. Melamine (99%), meta-phthalaldehyde (98%), para-phthalaldehyde (98%), and dimethyl sulfoxide (DMSO, purity >99%) were purchased from Aladdin Reagent Co., Ltd. and used as received.

2.2. Synthesis. The synthesis method via the Schiff base reaction was according to ref 40 (Scheme 1). Para-/meta-

Scheme 1. Formation of MBMOP-1 via the Schiff Base Reaction

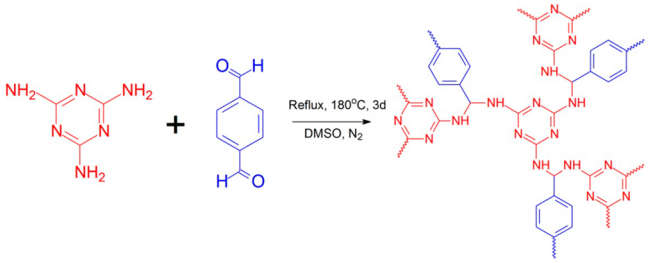

phthalaldehyde (1.61 g, 12.0 mmol), melamine (1.01 g, 8.0 mmol), and anhydrous DMSO (100 mL) were mixed in a 250 mL three-neck round-bottom flask equipped with a water-cooled condenser. After being purged with nitrogen several times, the mixture was heated to 453 K under vigorous stirring and kept at N_2 atmosphere for 72 h. Then the resultant mixture was cooled to room temperature. The white precipitate was collected by filtration and washed with vast amounts of acetone, tetrahydrofuran, and dichloromethane and finally dried at 353 K for 24 h in vacuum. The final product was presented as an off-white powder in 64% yield. The product was referred to as MBMOP-1 for para-phthalaldehyde and MBMOP-2 for meta-phthalaldehyde.

2.3. Characterization. Transmission electron microscopy (TEM) observations were carried out on a 2100 JEOL TEM working at 200 kV. The sample was diluted in ethanol to give a 1:5 volume ratio and sonicated for 10 min. The ethanol slurry was then dripped onto a Cu grid covered with a holey film of carbon. The SEM images were obtained using a HITACHI S-4800 microscope equipped with a field emission gun. The acceleration voltage was set to 5 kV. The samples were stuck on the observation platform and sprayed with gold vapor under high vacuum for about 20 s. The FT-IR spectra were recorded on a Nicole Nexus 670 spectrometer with a resolution of 4 cm^{-1} using the KBr compression method. Ar adsorption was measured at 87.4 K using a Quantachrome Autosorb-1 analyzer. Prior to the measurements, the samples were outgassed in vacuum at 473 K for 24 h. The specific surface area was calculated by the BET (Brunauer−Emmett−Teller) method from the isotherm data in a relative pressure range of 0.1−0.3.

2.4. Adsorption Equilibrium Measurements. CO_2 and N_2 adsorption measurements were performed at different temperatures on a Micromeritics ASAP 2020 coupled with a recirculating water bath. The sample cell was loaded with ∼250 mg of the sorbent. After the sorbent was outgassed in vacuum at 393 K for 12 h, the adsorption run was carried out using high purity CO_2 (99.999%) and N_2 (99.99%) in a pressure range from 0.01 to 118 kPa.

All the CO_2 adsorption isotherms were fitted by the combined dual-site Langmuir (DSL) model:

$$q = q_{sat,1}\frac{b_1 p}{1 + b_1 p} + q_{sat,2}\frac{b_2 p}{1 + b_2 p} \quad (1)$$

where q is the amount adsorbed (mmol g^{-1}), p is the equilibrium pressure (kPa), $q_{sat,1}$ and $q_{sat,2}$ are the adsorption

dx.doi.org/10.1021/ie501736t | Ind. Eng. Chem. Res. 2014, 53, 11828−11837

capacity at site 1 and site 2 (mmol g^{-1}), respectively, and b_1 and b_2 are the equilibrium constants for site 1 and site 2 (kPa^{-1}).

The N_2 adsorption isotherms were fitted by the single site Langmuir (SSL) model:

$$q = q_{sat}\frac{bp}{1+bp} \quad (2)$$

Where q is the amount adsorbed (mmol g^{-1}), p is the equilibrium pressure (kPa), q_{sat} is the adsorption capacity (mmol g^{-1}). b is the equilibrium constant (kPa^{-1}).

The isosteric heats of adsorption Q_{iso} for CO_2 and N_2 on the samples are calculated by using the Clausius−Clapeyron equation

$$\left[\frac{Q_{iso}}{R}\right] = \left[\frac{\partial(\ln p)}{\partial(1/T)}\right]_\theta \quad (3)$$

The p value used is the analytical solution of correlated equation fitted by DSL or SSL as a function of amount adsorbed q.

The ideal selectivity on the basis of the fitted results is expressed as follows:

$$S = \frac{q_1 p_2}{q_2 p_1} \quad (4)$$

where q_1 and q_2 are the amounts adsorbed for components 1 and 2 and where p_1 and p_2 are the corresponding partial pressures, respectively.

2.5. Breakthrough Column Experiments. The breakthrough column experiments were carried out in a homemade apparatus equipped with a stainless steel tube with an inner diameter of 4.65 mm, an outer diameter of 6.35 mm, and a length of 10 cm, as illustrated schematically in Scheme S1 in Supporting Information. To minimize the possible pressure drop, the samples were compressed tablets and sieved to 30−40 mesh. The adsorbent was loaded to fill the sample tube. Both ends of the adsorption column were sealed with temperature-resistant glass wool to reduce the loss of adsorbent and the dead volume of system. Prior to the experiments, the adsorbent was purged by a He flow (20 mL/min) at 423 K for 12 h. Breakthrough separation experiments were conducted by flowing He−CO_2−N_2 mixtures with a total flow rate of 10 mL/min at 298 K and 1 bar. Different gas composition was obtained by altering the gas flow rate controlled by mass flow controllers. The He flow rate is always setting at 2 mL/min. A regeneration experiment was conducted by switching the gas mixture to He with a flow rate of 10 mL/min without changing the temperature.[44] Blank experiments were carried out using silica (20−40 mesh) with the same volume under the same conditions.

The dynamic adsorbed amount q_i was determined through integration of the experimental breakthrough curves, according to eq 5,[45]

$$q_i = \frac{1}{m_{sample}V_{mol}}\int_0^t \left[\left(\frac{F_{v,He,in}X_{i,out}}{(1-\sum_{i=1}^{N}X_{i,out})}\right)_{silica} - \left(\frac{F_{,v,He,in}X_{i,out}}{(1-\sum_{i=1}^{N}X_{i,out})}\right)_{sample}\right]dt \quad (5)$$

where m_{sample} is the mass of sample used, $F_{v,He,in}$ is the given flow of He, $X_{i,out}$ is the molar fraction of component i in the gas phase, and t is the first moment of the breakthrough curve of component i leaving the column.

2.6. CO_2 Adsorption Uptakes. The adsorption uptakes were obtained on a thermogravimetric analyzer (NETZSCH STA449). The sample cell (a dense alumina crucible pot) was loaded with ~15 mg of adsorbent. Prior to the CO_2 adsorption experiments, the adsorbent was pretreated at 423 K for 1 h in a He flow of 40 mL/min. After the sample was cooled to 298 K, the He flow was switched to a mixture flow containing 20% CO_2 and 80% N_2 for adsorption. The total feed flow was always set at 40 mL/min. The adsorption of CO_2 was carried out for 30 min. Afterward, the feed gas stream was switched to a He or N_2 flow of 40 mL/min while the temperature was kept at 298 K for desorption. This desorption (regeneration) process lasted for 30 min. The combined process is defined as one adsorption−desorption (capture−regeneration) cycle.

3. RESULTS AND DISCUSSION

3.1. Physicochemical Properties. The FT-IR spectra (Figure 1) reveal absorption peaks of the quadrant (1546 cm^{-1})

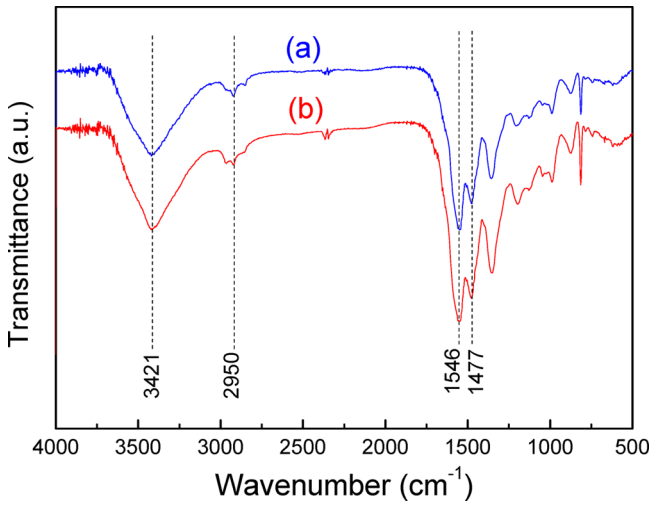

Figure 1. FT-IR spectra of the MBMOPs samples: (a) MBMOP-1 and (b) MBMOP-2.

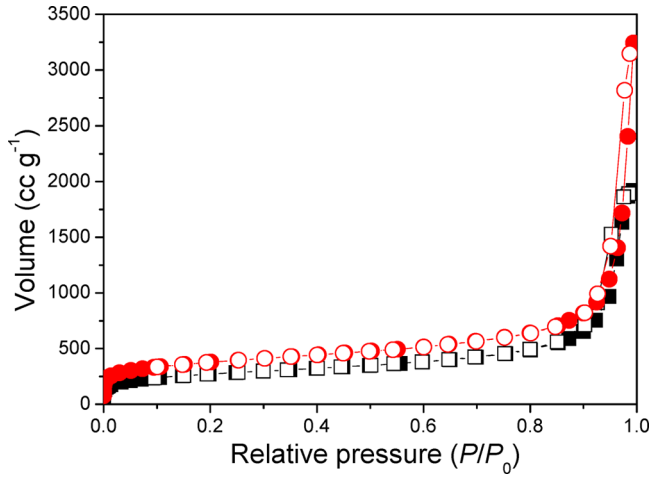

Figure 2. Ar adsorption−desorption isotherms at 87.4 K of MBMOP-1 (square plot) and MBMOP-2 (circle plot).

dx.doi.org/10.1021/ie501736t | Ind. Eng. Chem. Res. 2014, 53, 11828−11837

Table 1. Textural Properties of the Synthesized MBMOPs

sample	S_{BET} ($m^2\ g^{-1}$)	V_{total} ($cm^3\ g^{-1}$)[a]	V_{total} ($cm^3\ g^{-1}$)[b]	V_{micro} ($cm^3\ g^{-1}$)[c]	D_{pore} (nm)[d]
MBMOP-1	747	2.44	1.78	0.13	0.55
MBMOP-2	1082	4.13	1.57	0.22	0.50

[a]Total pore volume calculated from argon adsorption at $p/p_0 = 0.994$. [b]NLDFT pore volume for pores with diameter less than 25 nm. [c]NLDFT micropore volume for pores with diameter less than 1 nm. [d]Pore width calculated from NLDFT.

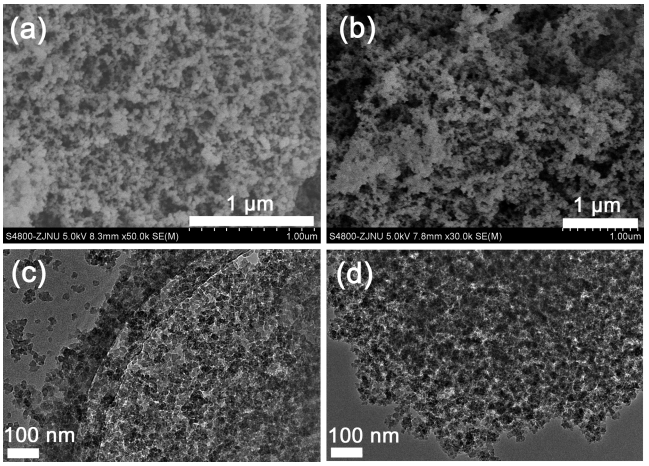

Figure 3. SEM (a, b) and TEM (c, d) images of the synthesized MBMOPs: (a, c) MBMOP-1 and (b, d) MBMOP-2.

and semicircle stretching (1477 cm^{-1}) of the triazine ring, indicating the successful incorporation of the melamine into the network. Bands of NH_2 stretching (3470 and 3420 cm^{-1}) and NH_2 deformation (1650 cm^{-1}) attributed to the residual primary amine group of melamine as well as C−H stretching (2720 cm^{-1}) and C═O stretching (1700 cm^{-1}) attributed to the carbonyl signals of phthalaldehyde are absent or strongly attenuated in the spectra of the MBMOPs (Figure S1). No obvious band around 1600 cm^{-1} corresponding to the C−N stretching vibration is observed in the FT-IR spectrum of the network. FT-IR confirms the formation of the melamine based polymer as well as a deep extent of polymerization.

Argon adsorption isotherms at 87.4 K of the synthesized MBMOPs display a combination of type I and type II profile, indicating the presence of both micropores and meso-/macropores (Figures 2 and S2). The porosity parameters are summarized in Table 1. The MBMOPs exhibit high specific surface areas, which are 747 and 1082 $m^2\ g^{-1}$ for MBMOP-1 and MBMOP-2, respectively. Total pore volumes of MBMOP-1 and MBMOP-2 determined from Ar adsorption at relative pressure $P/P_0 = 0.99$ are as large as 2.44 and 4.13 $cm^3\ g^{-1}$, respectively. Nevertheless, one can observe that very steep climbs are present on isotherms at relative pressure ranging from 0.95 to 0.99, especially for MBMOP-2, as a consequence of Ar condensation in voids or external surfaces. In order to eliminate the interference of Ar condensation, the NLDFT cumulative pore volume for pores with diameter less than 25

Table 2. Estimated Values of Adsorption Parameters and 95% Confidence Limits for the Combined Fitting of the Isotherm Data of CO_2 on MBMOP-1 with a DSL Model

	first site		second site	
temp (K)	$q_{sat,1}$ ($mmol\ g^{-1}$)	b_1 ($\times10^{-3}\ kPa^{-1}$)	$q_{sat,2}$ ($mmol\ g^{-1}$)	b_2 ($\times10^{-3}\ kPa^{-1}$)
298	0.51 ± 0.02	83.0 ± 4.0	3.18 ± 0.03	5.55 ± 0.22
323	0.51 ± 0.02	23.5 ± 0.76	3.18 ± 0.03	2.61 ± 0.95
348	0.51 ± 0.02	9.34 ± 0.24	3.18 ± 0.03	1.46 ± 0.05

Table 3. Estimated Values of Adsorption Parameters and 95% Confidence Limits for the Combined Fitting of the Isotherm Data of CO_2 on MBMOP-2 with a DSL Model

	first site		second site	
temp (K)	$q_{sat,1}$ ($mmol\ g^{-1}$)	b_1 ($\times10^{-3}\ kPa^{-1}$)	$q_{sat,2}$ ($mmol\ g^{-1}$)	b_2 ($\times10^{-3}\ kPa^{-1}$)
298	0.62 ± 0.04	90.3 ± 6.7	2.96 ± 0.03	7.37 ± 0.43
323	0.62 ± 0.04	27.3 ± 1.5	2.96 ± 0.03	3.41 ± 0.18
348	0.62 ± 0.04	11.3 ± 0.5	2.96 ± 0.03	1.83 ± 0.09

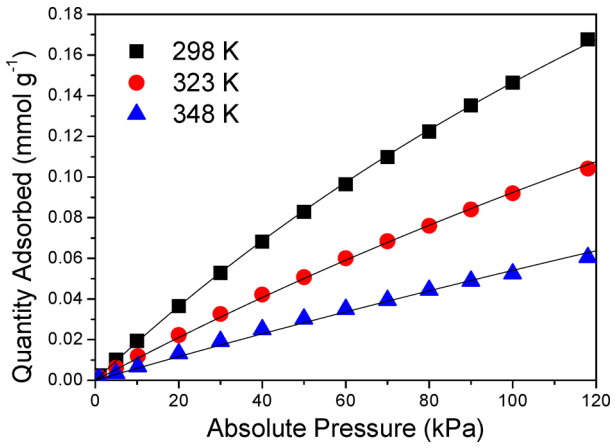

Figure 5. Adsorption isotherms of N_2 on MBMOP-1 at different temperatures. Symbols are the experimental data, and lines are the combined SSL model correlations.

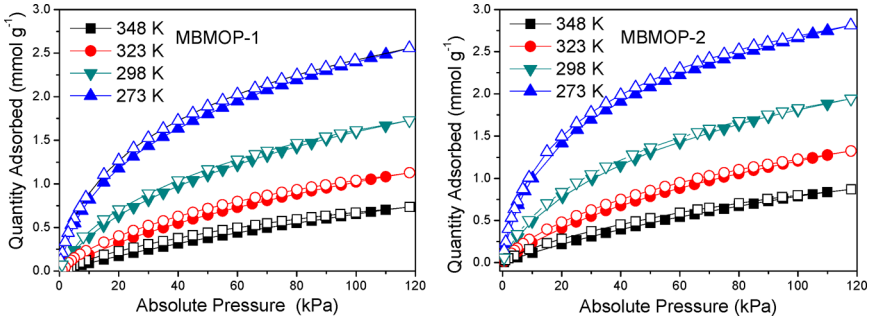

Figure 4. CO_2 adsorption isotherms of MBMOP-1 and MBMOP-2.

dx.doi.org/10.1021/ie501736t | Ind. Eng. Chem. Res. 2014, 53, 11828−11837

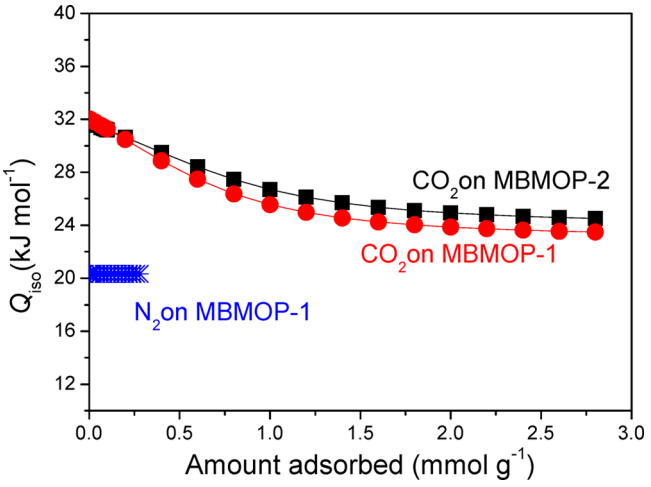

Figure 6. Isosteric heat of adsorption as a function of fractional occupancy for CO_2 and N_2 on MBMOPs.

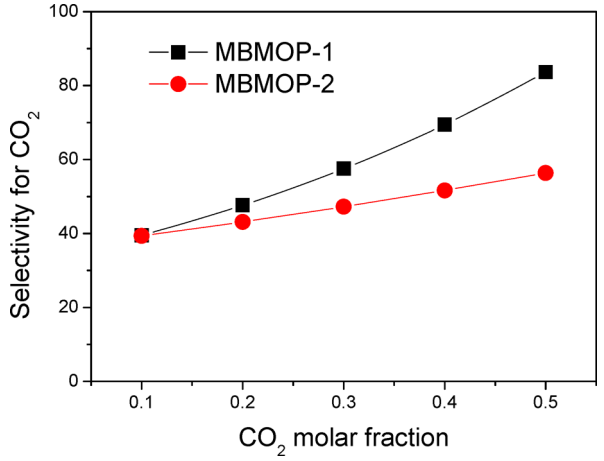

Figure 7. Ideal selectivity for CO_2 over N_2 as a function of CO_2 molar fraction on MBMOPs at 298 K and a total pressure of 100 kPa.

nm was taken as the DFT total pore volume. As shown in Table 1, MBMOP-1 has a DFT pore volume of 1.78 cm^3 g^{-1} larger than MBMOP-2 (1.57 cm^3 g^{-1}). On the other hand, the latter has a larger DFT the micropore volume, indicating that MBMOP-2 possesses more abundant microporosity. The pore widths determined by the NLDFT method are 0.55 and 0.50 nm for MBMOP-1 and MBMOP-2, respectively. Additionally, the multiple peaks in the DFT pore size distributions suggest that the synthesized MBMOPs possess an intricate microporous system (Figure S3).

The synthesized MBMOPs display a good thermal stability. No decomposition is observed at temperatures below 523 K in air atmosphere (Figure S4). As demonstrated in SEM images, the skeleton of MBMOPs consists of homogeneously interconnected particles, producing the meso-/macroporous voids evidenced by the Ar adsorption. The homogeneity of particle size (20−30 nm) and texture of MBMOPs are also confirmed by the TEM observations (Figure 3).

3.2. Pure Gas Adsorption. The single component sorption properties of MBMOPs were investigated by measuring sorption isotherms using the volumetric method. Figure 4 shows the CO_2 sorption isotherms on MBMOPs, which are type I according to the IUPAC classification. Additionally, the isotherms of CO_2 on MBMOPs are almost reversible over the entire pressure and temperature range investigated, implying that the adsorbed CO_2 on MBMOPs can be desorbed by a sole reduction of pressure. The adsorbed amount of CO_2 on MBMOP-1 is 2.56 mmol g^{-1} at 273 K and 118 kPa, while the value increases to 2.81 mmol g^{-1} for MBMOP-2. The CO_2 adsorption capacities are among the highest level in comparison with that on other MOPs, as reported in Table S2. The enhanced adsorption amount could be attributed to the larger surface area and micropore volume of MBMOP-2. As expected, the adsorption amount decreases as temperature increases. Nevertheless, the adsorption amount still is 0.73 and 0.87 mmol g^{-1} at 348 K for MBMOP-1 and MBMOP-2, respectively, showing the good CO_2 capture properties at elevated temperatures.

Polar groups have been reported to have more potential to increase the amount of CO_2 adsorbed.[46] In the synthesized MBMOPs, melamine, as building block, brings amine groups, which show good affinity with CO_2 molecules. The amine groups located at different areas, e.g., micropores and macropores, would present variety in CO_2 adsorption potential. As can be seen in Figure 4, the isotherms slightly bend to the vertical axis at pressures lower than 60 kPa while the isotherms become approximately linear at pressures exceeding 60 kPa. The subtle inflections on the isotherms suggest the occurrence of multisite adsorption for CO_2 on MBMOPs, which has also been reported for other conjugated microporous polymers by Dawson et al.[46] For the sake of simplification, the adsorption sites are classified into two types: amine functionalized groups in micropores and those outside micropores. On the basis of the above considerations, the DSL model (eq 1) has been attempted to describe the adsorption equilibria of CO_2 on MBMOPs.[38] The saturated adsorption capacity q_{sat} should remain constant, since the thermal expansion of the adsorbed phase can be negligible in the temperature range investigated.[47] Nonlinear parameter estimation was carried out using a combined fitting method in which the q_{sat} values were shared for different temperatures. The measured isotherm data on MBMOPs can be appropriately correlated with the combined DSL model (Figure S5), and the corresponding estimated values of adsorption parameters are collected in Tables 2 and 3. The adsorption equilibrium constant for the first site (b_1) is significantly larger than that for the second site (b_2) at all temperatures, implying a much stronger affinity for CO_2 on site 1 than on site 2. The contribution of site 1 and site 2 to the CO_2 adsorption on MBMOPs based on the fitting data is illustrated in Figure S6. CO_2 dominantly adsorbs on site 1 at low pressures and achieves adsorption saturation at about 20 kPa. On the other hand, the amount adsorbed on site 2 still accumulates with the increase of the pressure (Figure S7). It can be deduced that CO_2 adsorption on site 1 is attributed to the micropore filling while that on site 2 mainly comes from adsorption on other pores except for micropres. For all the adsorption of CO_2 on both sites, the b values for MBMOP-2 are a bit larger than that for MBMOP-1.

The adsorption isotherms of N_2 on MBMOP-1 are shown in Figure 5. Compared with the adsorption of CO_2, the adsorption amount of N_2 on MBMOP-1 is fairly low. No discernible inflections are observed on isotherms for N_2, and the SSL model (eq 2) is enough to describe the isotherm data.[38] As shown in Figure 4, the N_2 adsorption isotherms are well fitted with the SSL model. The corresponding extracted values of the adsorption parameters are listed in Table S1. The estimated saturated adsorption capacities and equilibrium constants for

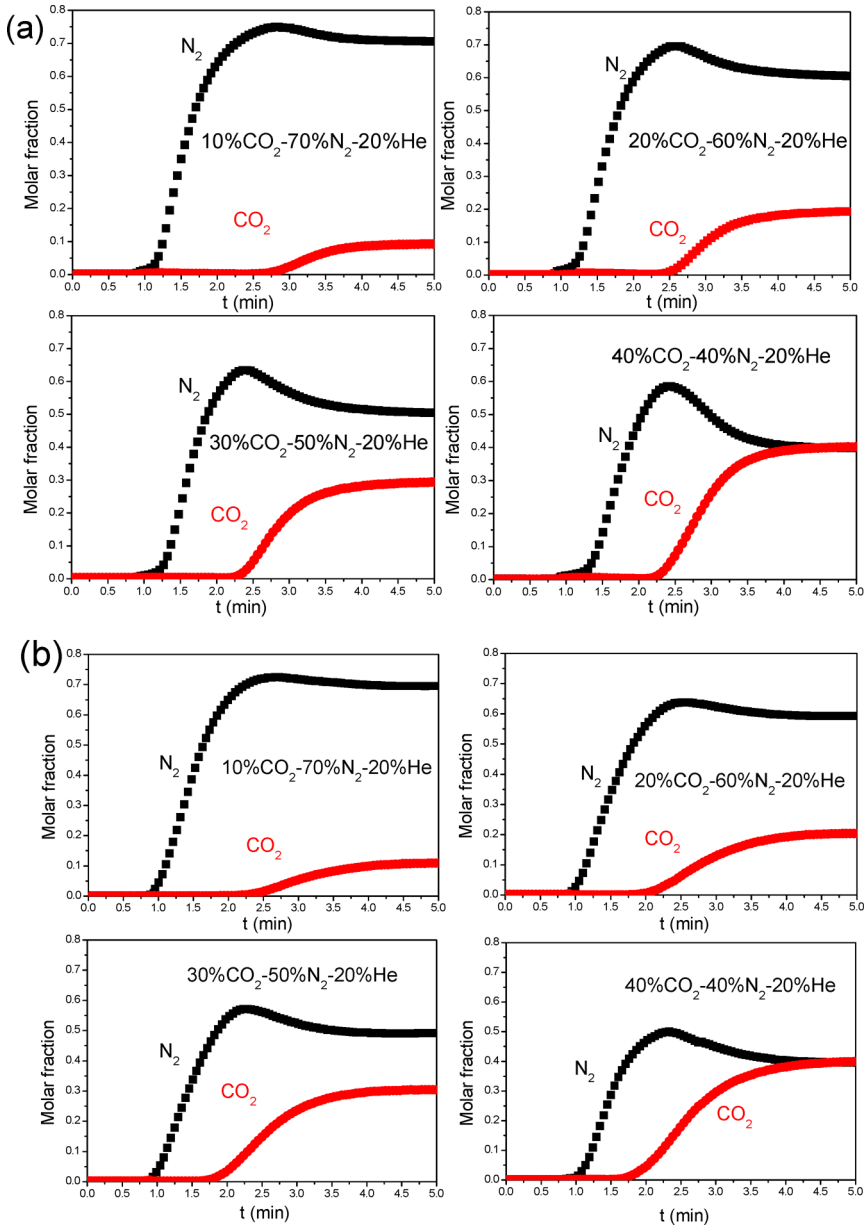

Figure 8. Breakthrough curves of CO_2–N_2 mixtures on (a) MBMOP-1 and (b) MBMOP-2 at 298 K and different CO_2 molar fractions. Mass of MBMOP-1and MBMOP-2 is 0.22 and 0.18 g, respectively.

both N_2 are much lower than those for the CO_2, implying the preferential adsorption of CO_2 over N_2 on MBMOPs.

3.3. Isosteric Heat of Adsorption. The isosteric adsorption technique was used to calculate the heats of adsorption to provide information about the interaction between the adsorptives and the adsorbent surfaces. The isosteric heats of adsorption, Q_{iso} (kJ mol^{-1}), were calculated from the adsorption isotherms at different temperatures by using the Clausius–Clapeyron equation (eq 3). The curves of Q_{iso} versus adsorption amount are shown in Figure 6. All calculated values of isosteric heat of adsorption are higher than the corresponding heat of vaporization of adsorbates (15.33 and 5.55 kJ mol^{-1} for CO_2 and N_2), indicating a high adsorption potential between the inner surface of MBMOPs and gas molecules. Overall, CO_2 has a higher isosteric of adsorption heat than N_2, suggesting the stronger affinity of CO_2 on both MBMOPs. The Q_{iso} for CO_2 on both MBMOPs are in the range of 24.1–32.2 kJ mol^{-1}, which are comparable to those obtained with the previously reported porous polymers.[39,46] With the increase of the surface coverage, Q_{iso} for CO_2 gradually decreases, while Q_{iso} levels off to about 24 kJ mol^{-1} when the CO_2 adsorbed amount exceeds 1.6 mmol g^{-1}. The variation of the isosteric heat indicates that the CO_2 adsorption on MBMOPs is energetically heterogeneous. Both of the adsorption equilibrium constant and the adsorption Q_{iso} for CO_2 on MBMOP-2 is higher than those on MBMOP-1, implying that the MBMOP-2 has a stronger adsorption potential for CO_2 than MBMOP-1. Q_{iso} for N_2 on MBMOP-1 is 20.3 kJ mol^{-1}, which is close to those values reported for some other porous polymers with high CO_2 selectivity.[39]

3.4. Binary Adsorption Prediction. The ideal adsorbed solution theory (IAST) developed by Myers and Prausnitz[48] is frequently utilized to predict multicomponent isotherms on the basis of single component isotherms. The binary gas IAST isotherms show a successive increment in the ideal selectivity (calculated by eq 4) for CO_2 over N_2 with an increase of the

dx.doi.org/10.1021/ie501736t | Ind. Eng. Chem. Res. 2014, 53, 11828–11837

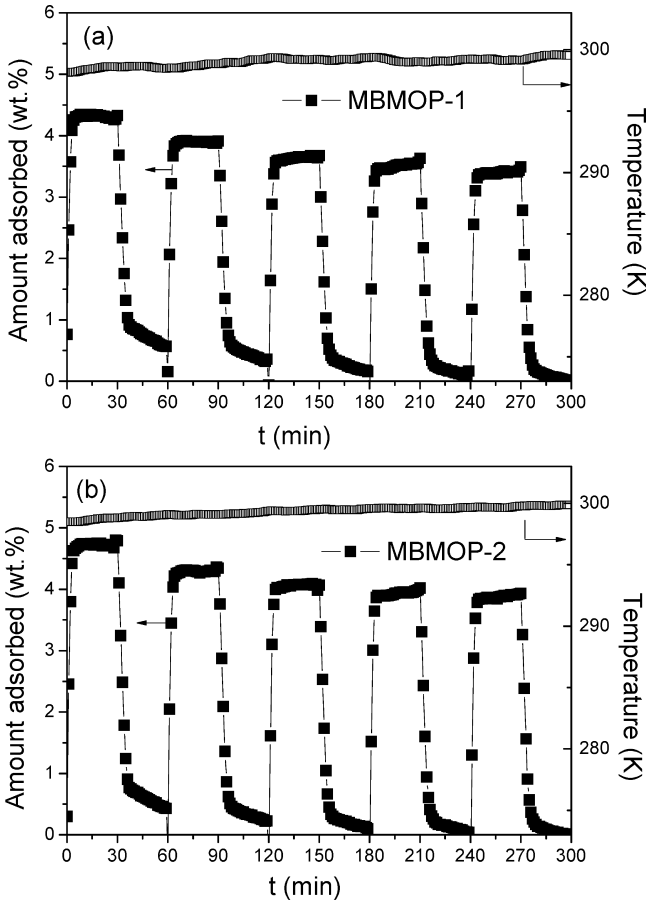

Figure 9. Five cycles of CO_2 adsorption−desorption on (a) MBMOP-1 and (b) MBMOP-2. The sample was pretreated at 423 K for 1 h in a He flow of 40 mL/min. Adsorption was in a mixture flow of 40 mL/min with CO_2 partial pressure of 0.2 bar, and regeneration was in a He flow of 40 mL/min. The adsorption and desorption temperature was always kept around 298 K.

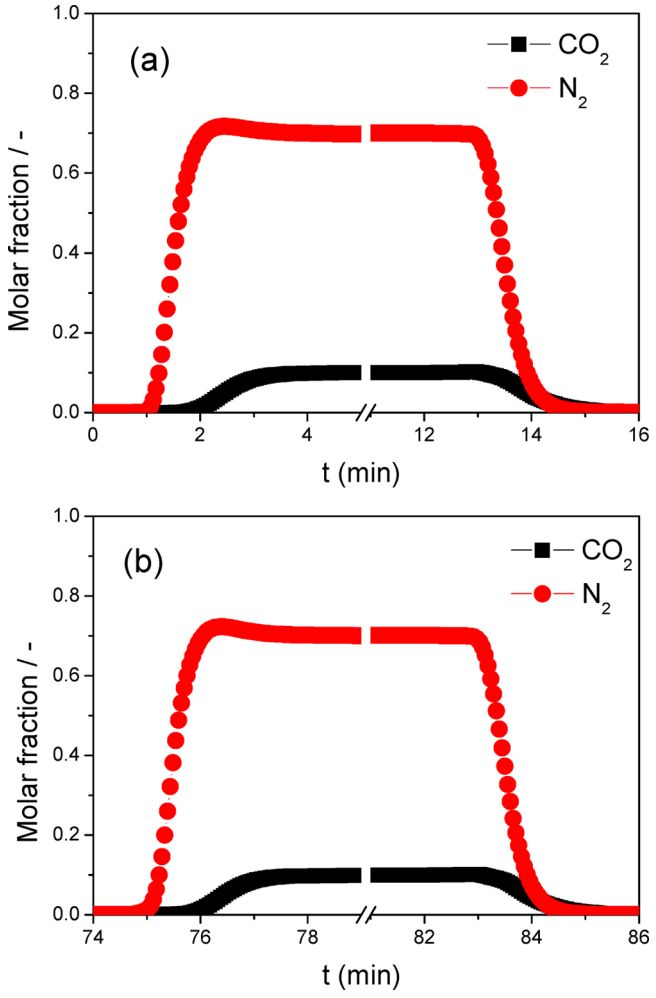

Figure 10. CO_2 capture−regeneration breakthrough curves on MBMOP-1 at 298 K and a CO_2 molar fraction of 0.1: (a) the first cycle and (b) the fifth cycle. Adsorbent used was 0.17 g.

total pressure at all CO_2 molar fractions investigated (Figures S8−S12). At a given total pressure of 100 kPa, the ideal selectivity for CO_2 over N_2 was plotted as a function of CO_2 molar fraction, as shown in Figure 7. On both MBMOPs, the selectivities for CO_2 increase in line with the CO_2 molar fraction. The predicted selectivity for CO_2 on MBMOP-1 ranges from 39.5 to 83.7 depending on the CO_2 molar fraction in CO_2−N_2 mixture, which is comparable to the values of selected porous polymers reported (Table S2). Unexpectedly, lower CO_2 selectivities on MBMOP-2 are observed compared with those on MBMOP-1, despite that the former has a stronger adsorption potential for CO_2. The reason is that MBMOP-2 also has a higher N_2 adsorption amount, which results in the reduction of the CO_2 selectivity (Figures S11, S12). The selectivity for CO_2 over N_2 on MBMOP-1 decreases when increasing the temperature (Figure S10), indicating that the high selectivity should not be ascribed to N_2 phobicity, which has been reported in the case of azo-COPs by Patel et al.[39] Despite this, the large amount of amines in MBMOPs contributes to high CO_2 adsorption selectivities over N_2 on MBMOPs.

3.5. Breakthrough Separation Experiments. To evaluate the dynamic CO_2 adsorption capacity and selectivity over N_2, breakthrough separation experiments with MBMOPs were conducted under different CO_2 partial pressures at 298 K.

Figure 8 shows the breakthrough curves of the CO_2−N_2 mixtures at 298 K and 1 bar on MBMOPs. At the beginning, only helium is detected while both of CO_2 and N_2 are retained in the column until the first component N_2 elutes from the column, indicating that N_2 is more weakly adsorbed. Under the investigated conditions, a complete separation of CO_2−N_2 mixtures can be achieved on either MBMOP-1 or MBMOP-2. A roll-up effect appears in the breakthrough curves of N_2, especially in curves for high CO_2 molar fractions. The roll-up effect may be attributed to the partial desorption of N_2 caused by the CO_2 competitive adsorption in the column. Another possible explanation is that the rapid desorption of N_2 results from a temperature wave caused by the exothermic adsorption of CO_2, suggested by Hamon et al.[49]

The dynamic adsorption amount data determined from breakthrough curves are collected in Table S3. The CO_2 amount adsorbed increases when increasing the CO_2 partial pressure, and the amount adsorbed at each CO_2 partial pressure coincide well with those from the equilibrium adsorption isotherms. Ascribed to the roll-up effect, it is hard to accurately determine the N_2 adsorbed amount. Nevertheless, overall MBMOP-2 exhibits a higher N_2 adsorption amount compared with MBMOP-1. As a result, MBMOP-2 has a lower CO_2 selectivity over N_2 than MBMOP-1, in accordance with the prediction of IAST (Figure S13).

dx.doi.org/10.1021/ie501736t | Ind. Eng. Chem. Res. 2014, 53, 11828−11837

3.6. Capture−Regeneration Properties. The gravimetric method is an efficient way to determine the gas adsorption uptakes over MBMOPs by monitoring the mass change caused by the gas adsorption.[50] As shown in Figure 9, both MBMOP-1 and MBMOP-2 exhibit a very fast uptake rate and the adsorption can reach an equilibrium within 4 min. More importantly, the rapid desorption can be achieved by only purging in a He flow rather than simultaneously raising the temperature as for regeneration of the conventional amine functionalized materials.[14,51] It should be pointed that the weight increment is caused by the adsorption of both CO_2 and N_2. The total adsorption equilibrium amount is very close to the sum of CO_2 and N_2 adsorption amount determined from the isotherms at the corresponding pressure, indicating that the adsorptive can be completely desorbed from MBMOPs by the He purging. Remarkably, the MBMOPs show an excellent stability, as demonstrated by 30 cycles of CO_2 adsorption−desorption (Figure S14).

The cycle performance of adsorption separation for CO_2−N_2 mixtures has also been examined by the breakthrough column technique. Almost no change of the gas adsorption and desorption behavior was observed during the five cycles (Figure S15). As indicated in the first cycle of CO_2 capture−regeneration (Figure 10a), N_2 outflows from the column prior to CO_2, illustrating the possibility of the separation of CO_2−N_2 mixture. During the regeneration period, gases adsorbed can be completely removed from MBMOPs by only purging in a He flow. The fifth cycle coincides well with the first one, demonstrating the excellent reversibility of adsorption on the MBMOP adsorbents under the regeneration conditions applied (Figure 10b).

The heat of adsorption for CO_2 on MBMOPs is 24−30 kJ mol^{-1}, which is close to that on an activated carbon (30 kJ mol^{-1}) and lower than that on 13X (36 kJ mol^{-1}) reported by Chue et al.[52] The lower value of the heat of adsorption on MBMOPs suggests that less energy is required for desorption. In practice, differing from the amine functionalized solid adsorbents, e.g., amine functionalized mesoporous silica,[14,16] MBMOPs can be easily regenerated by purging with a He flow, showing a promising prospect in the PSA processing.

4. CONCLUSIONS

Melamine based microporous organic polymers (MBMOPs) with abundant microporosity and plenty of amine groups have been successfully synthesized using melamine and phthalaldehyde as starting materials via the Schiff base reaction. The adsorption isotherms of CO_2 and N_2 on the prepared polymers have been accurately measured at pressures up to 118 kPa and temperatures ranging from 273 to 348 K, showing a high CO_2 adsorption amount of up to 2.8 mmol g^{-1} at 273 K and 118 kPa. The DSL model describes well the equilibrium data for CO_2 on MBMOPs. The dual site adsorption of CO_2 on MBMOPs is also illustrated by the piecewise linear function of the isosteric heat vs coverage. On the other hand, the N_2 adsorption isotherms on MBMOPs present fairly low capacities and can be well described by the SSL model. The mixture adsorption isotherms predicted by IAST suggest that high selectivities for CO_2 over N_2 are available on MBMOPs. The selectivity reaches 83.7 for equilimolar fraction and still maintains 39.5 even at 0.1 CO_2 molar fraction (CO_2−N_2). The high selectivities for CO_2 over N_2 were also confirmed by the breakthrough curves, on which CO_2 can be separated from the CO_2−N_2 mixtures. Remarkably, the adsorption capacities for CO_2 can be easily regenerated by He purging, implying the possibility of MBMOPs as high selective CO_2 adsorbents in the PSA process. The MBMOPs exhibit good stability, confirmed by 30 CO_2 adsorption−desorption cycles. Ascribed to the merits of high CO_2 adsorption capacities, high CO_2 selectivities, and good regeneration properties, MBMOPs as CO_2 adsorbents for the industrial separation of CO_2−N_2 mixture are highly anticipated.

■ ASSOCIATED CONTENT

Ⓢ Supporting Information

Schematic diagram of the breakthrough column setup, IR of monomers, Ar adsorption isotherms in log scale, pore size distribution, XRD, TG-DTA, combined fitting data of isotherms, IAST prediction data, table comparing the CO_2 capture capacity and selectivity of MBMOPs with others from literature, binary gas adsorption selectivity, and cycles of CO_2 adsorption−desorption. This material is available free of charge via the Internet at http://pubs.acs.org.

■ AUTHOR INFORMATION

Corresponding Author

*Tel: +86 579 82283457. Fax: +86 579 82282234. E-mail: xiaoq@zjnu.edu.cn.

Notes

The authors declare no competing financial interest.

■ ACKNOWLEDGMENTS

The financial support provided by Natural Science Foundation of China (Grants 21101139 and 21371152) is gratefully acknowledged. Q.X. thanks Martijn de Lange for constructive discussions and helpful language suggestions.

■ REFERENCES

(1) Song, C. Global Challenges and Strategies for Control, Conversion and Utilization of CO_2 for Sustainable Development Involving Energy, Catalysis, Adsorption and Chemical Processing. *Catal. Today* **2006**, *115* (1−4), 2−32.

(2) Yu, K. M. K.; Curcic, I.; Gabriel, J.; Tsang, S. C. E. Recent Advances in CO_2 Capture and Utilization. *ChemSusChem* **2008**, *1* (11), 893−899.

(3) Yang, H. Q.; Xu, Z. H.; Fan, M. H.; Gupta, R.; Slimane, R. B.; Bland, A. E.; Wright, I. Progress in Carbon Dioxide Seperation and Capture: A Review. *J. Environ. Sci.* **2008**, *20*, 14−27.

(4) Yang, J.; Yu, X.; Yan, J.; Tu, S.-T. CO_2 Capture Using Amine Solution Mixed with Ionic Liquid. *Ind. Eng. Chem. Res.* **2014**, *53* (7), 2790−2799.

(5) Choi, S.; Drese, J. H.; Jones, C. W. Adsorbent Materials for Carbon Dioxide Capture from Large Anthropogenic Point Sources. *ChemSusChem* **2009**, *2* (9), 796−854.

(6) Jing, Y.; Wei, L.; Wang, Y.; Yu, Y. Synthesis, Characterization and CO_2 Capture of Mesoporous SBA-15 Adsorbents Functionalized with Melamine-Based and Acrylate-Based Amine Dendrimers. *Microporous Mesoporous Mater.* **2014**, *183* (1), 124−133.

(7) He, Y. F.; Seaton, N. A. Heats of Adsorption and Adsorption Heterogeneity for Methane, Ethane, and Carbon Dioxide in MCM-41. *Langmuir* **2006**, *22* (3), 1150−1155.

(8) Liu, X. W.; Li, J. W.; Zhou, L.; Huang, D. S.; Zhou, Y. P. Adsorption of CO_2, CH_4 and N_2 on Ordered Mesoporous Silica Molecular Sieve. *Chem. Phys. Lett.* **2005**, *416* (4−6), 198−201.

(9) Lu, W.; Sculley, J. P.; Yuan, D.; Krishna, R.; Wei, Z.; Zhou, H. C. Polyamine-Tethered Porous Polymer Networks for Carbon Dioxide Capture from Flue Gas. *Angew. Chem., Int. Ed.* **2012**, *51* (30), 7480−7484.

(10) Xu, X. C.; Song, C. S.; Andresen, J. M.; Miller, B. G.; Scaroni, A. W. Preparation and Characterization of Novel CO_2 "Molecular Basket" Adsorbents Based on Polymer-Modified Mesoporous Molecular Sieve MCM-41. *Microporous Mesoporous Mater.* **2003**, *62* (1−2), 29−45.
(11) Rochelle, G. T. Amine Scrubbing for CO_2 Capture. *Science* **2009**, *325* (5948), 1652−1654.
(12) Vaidya, P. D.; Kenig, E. Y. CO_2 Alkanolamine Reaction Kinetics: A Review of Recent Studies. *Chem. Eng. Technol.* **2007**, *30* (11), 1467−1474.
(13) Favre, E. Carbon Dioxide Recovery from Post-Combustion Processes: Can Gas Permeation Membranes Compete with Absorption? *J. Membr. Sci.* **2007**, *294* (1−2), 50−59.
(14) Hao, S.; Xiao, Q.; Yang, H.; Zhong, Y.; Pepe, F.; Zhu, W. Synthesis and CO_2 Adsorption Property of Amino-Functionalized Silica Nanospheres with Centrosymmetric Radial Mesopores. *Microporous Mesoporous Mater.* **2010**, *132* (3), 552−558.
(15) Yue, M. B.; Chun, Y.; Cao, Y.; Dong, X.; Zhu, J. H. CO_2 Capture by As-Prepared SBA-15 with an Occluded Organic Template. *Adv. Funct. Mater.* **2006**, *16* (13), 1717−1722.
(16) Feng, X.; Hu, G.; Hu, X.; Xie, G.; Xie, Y.; Lu, J.; Luo, M. Tetraethylenepentamine-Modified Siliceous Mesocellular Foam (MCF) for CO_2 Capture. *Ind. Eng. Chem. Res.* **2013**, *52* (11), 4221−4228.
(17) Hao, S.; Chang, H.; Xiao, Q.; Zhong, Y.; Zhu, W. One-Pot Synthesis and CO_2 Adsorption Properties of Ordered Mesoporous SBA-15 Materials Functionalized with APTMS. *J. Phys. Chem. C* **2011**, *115* (26), 12873−12882.
(18) Herm, Z. R.; Swisher, J. A.; Smit, B.; Krishna, R.; Long, J. R. Metal-Organic Frameworks as Adsorbents for Hydrogen Purification and Precombustion Carbon Dioxide Capture. *J. Am. Chem. Soc.* **2011**, *133* (15), 5664−5667.
(19) An, J.; Geib, S. J.; Rosi, N. L. High and Selective CO_2 Uptake in a Cobalt Adeninate Metal-Organic Framework Exhibiting Pyrimidine- and Amino-Decorated Pores. *J. Am. Chem. Soc.* **2010**, *132* (1), 38−39.
(20) Yang, Q.; Zhong, C.; Chen, J. F. Computational Study of CO_2 Storage in Metal-Organic Frameworks. *J. Phys. Chem. C* **2008**, *112* (5), 1562−1569.
(21) Millward, A. R.; Yaghi, O. M. Metal−Organic Frameworks with Exceptionally High Capacity for Storage of Carbon Dioxide at Room Temperature. *J. Am. Chem. Soc.* **2005**, *127* (51), 17998−17999.
(22) Samanta, A.; Zhao, A.; Shimizu, G. K. H.; Sarkar, P.; Gupta, R. Post-Combustion CO_2 Capture Using Solid Sorbents: A Review. *Ind. Eng. Chem. Res.* **2012**, *51* (4), 1438−1463.
(23) Fracaroli, A. M.; Furukawa, H.; Suzuki, M.; Dodd, M.; Okajima, S.; Gándara, F.; Reimer, J. A.; Yaghi, O. M. Metal−Organic Frameworks with Precisely Designed Interior for Carbon Dioxide Capture in the Presence of Water. *J. Am. Chem. Soc.* **2014**, *136* (25), 8863−8866.
(24) Llewellyn, P. L.; Bourrelly, S.; Serre, C.; Vimont, A.; Daturi, M.; Hamon, L.; De Weireld, G.; Chang, J.-S.; Hong, D. Y.; Kyu Hwang, Y.; Hwa Jhung, S.; Ferey, G. High Uptakes of CO_2 and CH_4 in Mesoporous Metal Organic Frameworks MIL-100 and MIL-101. *Langmuir* **2008**, *24* (14), 7245−7250.
(25) Boutin, A.; Couck, S.; Coudert, F.-X.; Serra-Crespo, P.; Gascon, J.; Kapteijn, F.; Fuchs, A. H.; Denayer, J. F. M. Thermodynamic Analysis of the Breathing of Amino-Functionalized MIL-53(Al) upon CO_2 Adsorption. *Microporous Mesoporous Mater.* **2011**, *140* (1−3), 108−113.
(26) Stavitski, E.; Pidko, E. A.; Couck, S.; Remy, T.; Hensen, E. J. M.; Weckhuysen, B. M.; Denayer, J.; Gascon, J.; Kapteijn, F. Complexity Behind CO_2 Capture on NH_2-MIL-53(Al). *Langmuir* **2011**, *27* (7), 3970−3976.
(27) Zhang, Z.; Zhao, Y.; Gong, Q.; Li, Z.; Li, J. MOFs for CO_2 Capture and Separation from Flue Gas Mixtures: The Effect of Multifunctional Sites on Their Adsorption Capacity and Selectivity. *Chem. Commun.* **2012**, *49* (7), 653−661.
(28) Ben, T.; Ren, H.; Ma, S.; Cao, D.; Lan, J.; Jing, X.; Wang, W.; Xu, J.; Deng, F.; Simmons, J. M.; Qiu, S.; Zhu, G. Targeted Synthesis of a Porous Aromatic Framework with High Stability and Exceptionally High Surface Area. *Angew. Chem., Int. Ed.* **2009**, *48* (50), 9457−9460.
(29) Ben, T.; Pei, C.; Zhang, D.; Xu, J.; Deng, F.; Jing, X.; Qiu, S. Gas Storage in Porous Aromatic Frameworks (PAFs). *Energy Environ. Sci.* **2011**, *4* (10), 3991−3999.
(30) Pei, C.; Ben, T.; Guo, H.; Xu, J.; Deng, F.; Xiang, Z.; Cao, D.; Qiu, S. Targeted Synthesis of Electroactive Porous Organic Frameworks Containing Triphenyl Phosphine Moieties. *Philos. Trans. R. Soc., A* **2013**, *371*, 2000 20120312.
(31) Jiang, J. X.; Su, F.; Trewin, A.; Wood, C. D.; Campbell, N. L.; Niu, H.; Dickinson, C.; Ganin, A. Y.; Rosseinsky, M. J.; Khimyak, Y. Z.; Cooper, A. I. Conjugated Microporous Poly(aryleneethynylene) Networks. *Angew. Chem., Int. Ed.* **2007**, *119* (45), 8728−8732.
(32) Xie, Y.; Wang, T. T.; Liu, X. H.; Zou, K.; Deng, W. Q. Capture and Conversion of CO_2 at Ambient Conditions by a Conjugated Microporous Polymer. *Nat. Commun.* **2013**, *4*, 1960.
(33) Côté, A. P.; Benin, A. I.; Ockwig, N. W.; O'Keeffe, M.; Matzger, A. J.; Yaghi, O. M. Porous, Crystalline, Covalent Organic Frameworks. *Science* **2005**, *310* (5751), 1166−1170.
(34) Dawson, R.; Stoeckel, E.; Holst, J. R.; Adams, D. J.; Cooper, A. I. Microporous Organic Polymers for Carbon Dioxide Capture. *Energy Environ. Sci.* **2011**, *4* (10), 4239−4245.
(35) Woodward, R. T.; Stevens, L. A.; Dawson, R.; Vijayaraghavan, M.; Hasell, T.; Silverwood, I. P.; Ewing, A. V.; Ratvijitvech, T.; Exley, J. D.; Chong, S. Y.; Blanc, F.; Adams, D. J.; Kazarian, S. G.; Snape, C. E.; Drage, T. C.; Cooper, A. I. Swellable, Water- and Acid-Tolerant Polymer Sponges for Chemoselective Carbon Dioxide Capture. *J. Am. Chem. Soc.* **2014**, *136* (25), 9028−9035.
(36) Lu, W.; Yuan, D.; Zhao, D.; Schilling, C. I.; Plietzsch, O.; Muller, T.; Brase, S.; Guenther, J.; Blumel, J.; Krishna, R.; Li, Z.; Zhou, H. Porous Polymer Networks: Synthesis, Porosity, and Applications in Gas Storage/Separation. *Chem. Mater.* **2010**, *22* (21), 5964−5972.
(37) Vishnyakov, A.; Ravikovitch, P. I.; Neimark, A. V. Molecular Level Models for CO_2 Sorption in Nanopores. *Langmuir* **1999**, *15* (25), 8736−8742.
(38) Lu, W. G.; Sculley, J. P.; Yuan, D. Q.; Krishna, R.; Zhou, H. C. Carbon Dioxide Capture from Air Using Amine-Grafted Porous Polymer Networks. *J. Phys. Chem. C* **2013**, *117* (8), 4057−4061.
(39) Patel, H. A.; Je, S. H.; Park, J.; Chen, D. P.; Jung, Y.; Yavuz, C. T.; Coskun, A. Unprecedented High-Temperature CO_2 Selectivity in N_2-Phobic Nanoporous Covalent Organic Polymers. *Nat. Commun.* **2013**, *4*, 1357.
(40) Schwab, M. G.; Fassbender, B.; Spiess, H. W.; Thomas, A.; Feng, X.; Müllen, K. Catalyst-Free Preparation of Melamine-Based Microporous Polymer Networks through Schiff Base Chemistry. *J. Am. Chem. Soc.* **2009**, *131* (21), 7216−7217.
(41) Schwab, M. G.; Crespy, D.; Feng, X.; Landfester, K.; Muellen, K. Preparation of Microporous Melamine-Based Polymer Networks in an Anhydrous High-Temperature Miniemulsion. *Macromol. Rapid Commun.* **2011**, *32* (22), 1798−1803.
(42) Liu, L.; Li, P.; Zhu, L.; Zou, R.; Zhao, Y. Microporous Polymelamine Network for Highly Selective CO_2 Adsorption. *Polymer* **2013**, *54* (2), 596−600.
(43) Xu, C.; Hedin, N. Synthesis of Microporous Organic Polymers with High CO_2-over-N_2 Selectivity and CO_2 Adsorption. *J. Mater. Chem. A* **2013**, *1* (10), 3406−3414.
(44) Ren, X.; Sun, T.; Hu, J.; Wang, S. Highly Enhanced Selectivity for the Separation of CH_4 over N_2 on Two Ultra-Microporous Frameworks with Multiple Coordination Modes. *Microporous Mesoporous Mater.* **2014**, *186*, 137−145.
(45) Peralta, D.; Chaplais, G.; Simon-Masseron, A.; Barthelet, K.; Chizallet, C.; Quoineaud, A. A.; Pirngruber, G. D. Comparison of the Behavior of Metal-Organic Frameworks and Zeolites for Hydrocarbon Separations. *J. Am. Chem. Soc.* **2012**, *134* (19), 8115−8126.
(46) Dawson, R.; Adams, D. J.; Cooper, A. I. Chemical Tuning of CO_2 Sorption in Robust Nanoporous Organic Polymers. *Chem. Sci.* **2011**, *2* (6), 1173−1177.

(47) Zhu, W.; Groen, J. C.; van Miltenburg, A.; Kapteijn, F.; Moulijn, J. A. Comparison of Adsorption Behaviour of Light Alkanes and Alkenes on Kureha Activated Carbon. *Carbon* **2005**, *43* (7), 1416−1423.
(48) Myers, A. L.; Prausnitz, J. M. Thermodynamics of Mixed-Gas Adsorption. *AIChE J.* **1965**, *11* (1), 121−127.
(49) Hamon, L.; Jolimaître, E.; Pirngruber, G. D. CO_2 and CH_4 Separation by Adsorption Using Cu-BTC Metal-Organic Framework. *Ind. Eng. Chem. Res.* **2010**, *49* (16), 7497−7503.
(50) Xiao, Q.; Liu, Y. F.; Zhong, Y. J.; Zhu, W. D. A Citrate Sol-Gel Method to Synthesize Li_2ZrO_3 Nanocrystals with Improved CO_2 Capture Properties. *J. Mater. Chem.* **2011**, *21* (11), 3838−3842.
(51) Qi, G.; Fu, L.; Choi, B. H.; Giannelis, E. P. Efficient CO_2 Sorbents Based on Silica Foam with Ultra-Large Mesopores. *Energy Environ. Sci.* **2012**, *5* (6), 7368−7375.
(52) Chue, K. T.; Kim, J. N.; Yoo, Y. J.; Cho, S. H.; Yang, R. T. Comparison of Activated Carbon and Zeolite 13X for CO_2 Recovery from Flue Gas by Pressure Swing Adsorption. *Ind. Eng. Chem. Res.* **1995**, *34* (2), 591−598.